The potential of the greenness and radiation (GR) model to interpret 8-day gross primary production of vegetation

Chaoyang Wu [a,b,*], Alemu Gonsamo [b], Fangmin Zhang [c], Jing M. Chen [b]

[a] State Key Laboratory of Remote Sensing Science, Institute of Remote Sensing and Digital Earth, Chinese Academy of Sciences, Beijing, China
[b] Department of Geography, University of Toronto, 100 St. George St., Toronto, ON M5S 3G3, Canada
[c] Jiangsu Key Laboratory of Agricultural Meteorology, College of Applied Meteorology, Nanjing University of Information Science and Technology, Nanjing, Jiangsu 210044, China

ABSTRACT

Remote sensing of vegetation gross primary production (GPP) is an important step to analyze terrestrial carbon (C) cycles in response to changing climate. The availability of global networks of C flux measurements provides a valuable opportunity to develop remote sensing based GPP algorithms and test their performances across diverse regions and plant functional types (PFTs). Using 70 global C flux measurements including 24 non-forest (NF), 17 deciduous forest (DF) and 29 evergreen forest (EF), we present the evaluation of an upscaled remote sensing based greenness and radiation (GR) model for GPP estimation. This model is developed using enhanced vegetation index (EVI) and land surface temperature (LST) from the Moderate Resolution Imaging Spectroradiometer (MODIS) and global course resolution radiation data from the National Center for Environmental Prediction (NCEP). Model calibration was achieved using statistical parameters of both EVI and LST fitted for different PFTs. Our results indicate that compared to the standard MODIS GPP product, the calibrated GR model improved the GPP accuracy by reducing the root mean square errors (RMSE) by 16%, 30% and 11% for the NF, DF and EF sites, respectively. The standard MODIS and GR model intercomparisons at individual sites for GPP estimation also showed that GR model performs better in terms of model accuracy and stability. This evaluation demonstrates the potential use of the GR model in capturing short-term GPP variations in areas lacking ground measurements for most of vegetated ecosystems globally.

© 2013 International Society for Photogrammetry and Remote Sensing, Inc. (ISPRS) Published by Elsevier B.V. All rights reserved.

1. Introduction

Gross primary production (GPP) represents the gross carbon (C) fixed by terrestrial ecosystems through photosynthesis, which in turn drives several ecosystem functions (Beer et al., 2010). Therefore, accurate estimation of GPP can be a great advantage for quantifying net ecosystem production (NEP) and thus of particular importance for global C cycle research (Zhao and Running, 2010).

Remote sensing technique offers a unique tool for monitoring land surface globally and timely and hence several algorithms are proposed to estimate GPP based on a combination of remote sensing observations and ground measurements (Field et al., 1998; Zhao et al., 2005, 2006; Yuan et al., 2010; Wu et al., 2009). The main concept for estimating GPP from remote sensing observations is based on the Monteith (1972) logic,

$$GPP = LUE \times APAR \tag{1}$$

where LUE represents the light use efficiency, and APAR is the absorbed photosynthetically active radiation calculated as the product of an absorbed fraction (f_{APAR}) and the amount of incident photosynthetically active radiation (PAR).

Following Monteith's equation, GPP can be determined by estimating LUE and APAR separately and such method has shown promising results in designing satellite-based GPP models (e.g., the Moderate Resolution Imaging Spectroradiometer (MODIS) GPP products, Zhao et al., 2005; and the Vegetation Photosynthesis Model (VPM), Xiao et al., 2005). Vegetation indices (VIs), which provide measures of surface canopy greenness and vegetation status, are the most widely used metrics in driving remote sensing GPP models. A number of VIs have been shown to be useful in estimating GPP, including the normalized difference vegetation index (NDVI) (Rouse et al., 1974), the enhanced vegetation index (EVI) (Huete et al., 2002), the MERIS Terrestrial Chlorophyll Index (MTCI) (Dash and Curran, 2004), the land surface water index (Xiao et al., 2005) and the wide dynamic range vegetation index (WDRVI) (Gitelson, 2004). These VIs are incorporated in many existing GPP models, either independently (Gitelson et al., 2008; Harris and Dash, 2010; Kalfas et al., 2011) or in combination with other

* Corresponding author at: Department of Geography, University of Toronto, 100 St. George St., Toronto, ON M5S 3G3, Canada. Tel.: +1 647 524 0310.
E-mail address: hefery@163.com (C. Wu).

variables (e.g., temperature and evaporation) (Xiao et al., 2006; Coops et al., 2007; Gitelson et al., 2006; Sims et al., 2008; Hilker et al., 2008a; Zhang et al., 2009; Sakamoto et al., 2011; Wu et al., 2011; Peng and Gitelson, 2012).

One of the main sources of uncertainties in remote sensing based GPP models is the uncertainty in the LUE calculation, which is often achieved by an empirically determined maximum LUE for a specific land cover type. Climate variables are used to modulate the fixed values of land cover specific maximum LUE (Running et al., 2004). However, the dependence on input climate variables and the fact that each biome is assigned a single maximum LUE value can cause significant deviation of estimated GPP from observations (Zhao et al., 2006; Kanniah et al., 2009; Mu et al., 2011). In particular, spatiotemporal variations of LUE is a challenging issue for such models and increasing evidence shows that misinterpreting the spatiotemporal characteristics of LUE would significantly affect the modeled GPP (Turner et al., 2003; Wang et al., 2010). To compensate the empirically determined LUE, specific indicators are proposed to track LUE changes and thereby mitigating the dependence on input climate variables. For example, the photochemical reflectance index (PRI) (Gamon et al., 1997) has been demonstrated to have certain potential in estimating LUE. However, satellite determination of LUE using PRI alone is confounded by the canopy structure and the view observer geometry (Hilker et al., 2008b; Hall et al., 2011).

Recent studies have turned to other alternative models instead of the LUE concept for the estimation of GPP. For example, the temperature and greenness (TG) model proposed by Sims et al. (2008) that combines MODIS EVI and LST has shown good potential in modeling GPP for North America ecosystems. In particular, Gitelson et al. (2006) developed a chlorophyll content based GPP model in crops that predicts GPP using only two input parameters, i.e., chlorophyll index and incoming PAR. Later analysis showed that this model can provide better GPP estimates than that of the TG model for several flux sites in North America, including both deciduous forest and evergreen forests (Wu et al., 2011). However, there are two main difficulties for the application of such model for operational use. The first is the radiation data that are used to run the model. Most of the previous evaluations of this model used radiation data from site level meteorological measurements (Wu et al., 2010, 2011; Kalfas et al., 2011; Peng et al., 2011). Therefore, it would be difficult to explicitly compare the model estimates with the standard MODIS GPP product that uses coarse resolution radiation data since evidence has shown that the uncertainty in radiation will significantly affect the GPP outputs (Sakamoto et al., 2011). A second difficulty is the feasibility of the model for estimating and modeling short-term GPP variations in globally diverse vegetation ecosystems. Understandings of such uncertainties are especially important for upscaling the algorithm to map regional and global GPP where ground observations are lacking. Here we present the interpretation of short-term (8-day) GPP estimates derived using remote sensing observations and global coarse resolution radiation data (biases are generally within 50 W/m^2 depending on regions) over 70 global C flux sites. These sites cover various PFTs and thus provide an opportunity to test the robustness of the model and to further develop upscaling strategies. Therefore, the objective of this study is the global calibration and validation of the greenness and radiation (GR) model with respect to different PFTs. Furthermore, we compare the performances of the GR model and the standard MODIS GPP product against the ground measurements.

2. Materials and methods

2.1. Study sites

We base our analysis on 70 representative C flux tower sites, covering various vegetation ecosystems with latitudes ranging from ~40°S to ~70°N and longitudes from ~140°E to ~130°W (Fig. 1). The rules for site selection were mainly regulated by the data availability (at least 2 years of continuous and complete data records), data quality (less than 30% of gap-filled data), availability of site-level meteorological data (radiation and temperature), and no recent disturbances (fire, insect and harvest). To analyze the influences of PFT on model simulations, we grouped the sites into three PFTs: 24 non-forest vegetation (NF) sites, 17 deciduous forests (DF) sites and 29 evergreen forest (EF) sites. Detailed descriptions of each site and their regional climates are shown in Supplementary Table 1.

2.2. Flux and meteorological data

The C flux data were downloaded from the following flux networks, AmeriFlux (http://public.ornl.gov/ameriflux/dataproducts.shtml), Fluxnet-Canada (www.fluxnet-canada.ca), EuroFlux (www.europe-fluxdata.eu), CarboAfrica (www.europe-fluxdata.
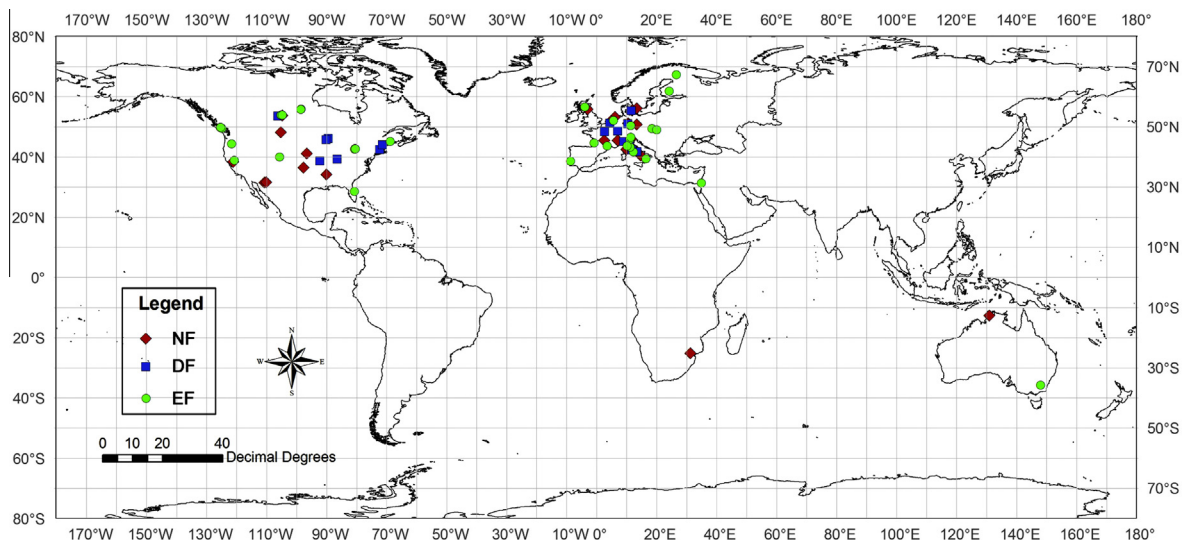

Fig. 1. Spatial distribution of the flux sites in this study, the NF (◆), DF (■), and EF (●) represent non-forest deciduous forest, and evergreen forest ecosystems, respectively.

eu/newtcdc2/CarboAfrica_home.aspx), and the Public FLUXNET Dataset Information (www.fluxdata.org).

Since these data were acquired from different regional flux networks, two gap-filling procedures were applied. For Fluxnet-Canada sites, the estimation of GPP and R_e were achieved by empirical relationships: (1) nighttime NEE and nighttime temperature and (2) daytime GPP and PAR. The procedures for gap-filling were described in Barr et al. (2004) which was the standard method for all Fluxnet-Canada sites. For sites from other regional flux networks, level-4 products were used which contain gap-filled and u^* (typically value of u^* was 0.35 m s^{-1} but may differ slightly for individual sites) filtered records of C fluxes with quality flags for both original and gap-filled data. The half-hourly measurements were gap-filled using the Artificial Neural Network (ANN) method
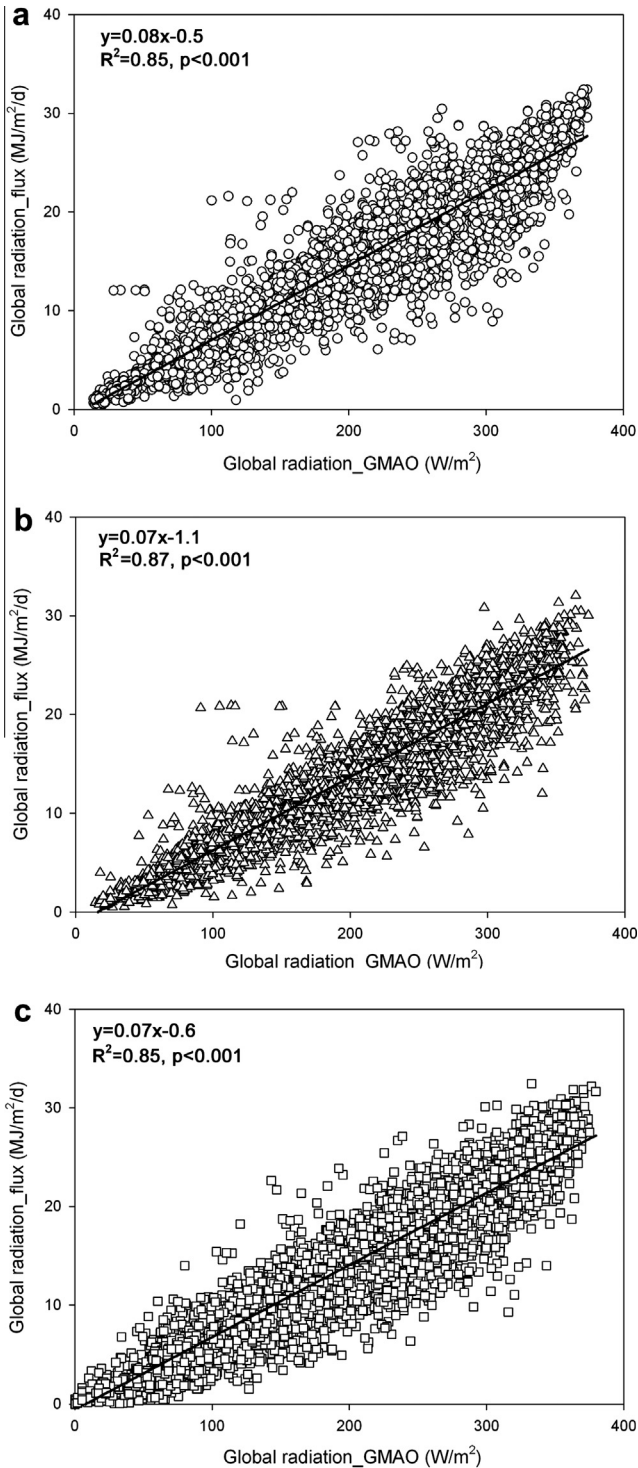

Fig. 2. Relationships between shortwave solar radiation acquired from the National Center for Environmental Prediction (NCEP) reanalysis II data and radiation of on site measurements. The NF (○), DF (△), and EF (□) represent non-forest, deciduous forest, and evergreen forest ecosystems, respectively.
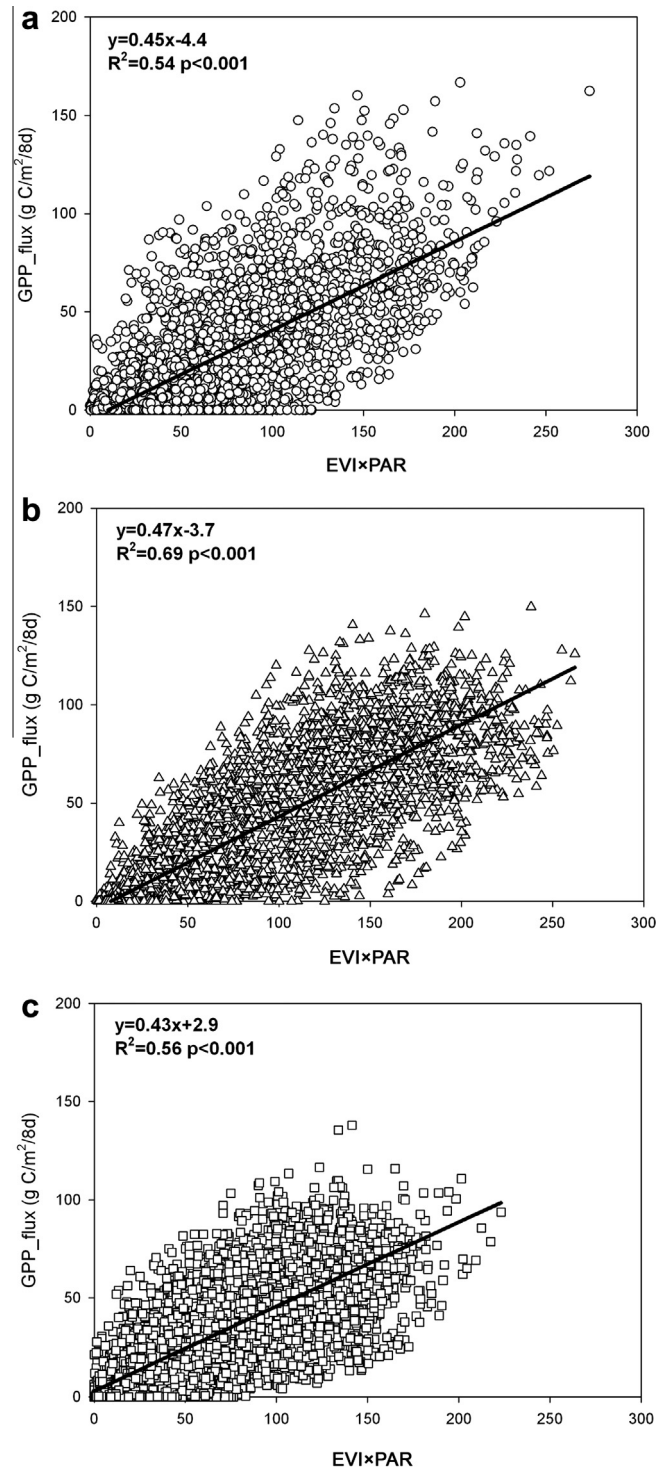
Fig. 3. Relationships between flux-measured 8 day gross primary production (GPP) and the product of enhanced vegetation index and photosynthetic radiation (EVI × PAR) for (a) non-forest (○), (b) deciduous forest (△), and (c) evergreen forest (□), respectively.

(Papale and Valentini, 2003) and/or the Marginal Distribution Sampling (MDS) method (Reichstein et al., 2005). Although different gap-filling methods were used, the reliability of multiple site comparisons and syntheses can be assumed as most methods tended to cluster on similar results to within 10% (Desai et al., 2008), which also agrees with the general understanding that biases associated with different gap filling methods tend to be small and supports our analysis across multiple sites (Papale et al., 2006). Apart from the aggregated 8-day composite of GPP, we also calculated the 8-day air temperature, global radiation and precipitation from the site meteorological measurements.

2.3. MODIS products

We used three MODIS land surface products in this study, which were acquired from the Oak Ridge National Laboratory's Distributed Active Archive Center (DAAC) website (http://daac.ornl.gov/MODIS/). The first product is the 8-day MODIS Terra Surface Reflectance Product (MOD09A1, 500 m, collection 5), which provides surface reflectances for seven bands centered at 648 nm, 858 nm, 470 nm, 555 nm, 1240 nm, 1640 nm, and 2130 nm (Vermote et al., 1997). Pixels that are contaminated by cloud and aerosol were removed using the quality flag and only good data were selected. Reflectance was extracted from 3×3 MODIS pixels (1.5 km × 1.5 km) that centered on the flux tower, which is similar with previous analyses (Sims et al., 2008; Wu et al., 2011). Reflectances from three spectral bands, blue (R_{blue}), red (R_{red}), and near-infrared (R_{NIR}) were used to calculate the EVI as in Huete et al. (2002):

$$EVI = 2.5 \times \frac{R_{NIR} - R_{Red}}{1 + R_{NIR} + 6 \times R_{Red} - 7.5 \times R_{Blue}} \qquad (2)$$

We have not use the standard MODIS EVI product because the temporal resolution of that product is 16 days while our objective is to interpret 8-day GPP.

We also extracted MODIS 8-day Land Surface Temperature (LST) product (MOD11A2, 1 km, collection 5) derived by applying the generalized split-window algorithm. In the split-window algorithm, emissivity in bands 31 and 32 are estimated from land cover types, and atmospheric column water vapor and lower boundary air surface temperature are separated into tractable sub-ranges for optimal retrieval (Wan, 2008). The data quality was checked through the quality flag such that only good data in the original L1B data were used and LST contaminated by cloud effects and poor retrievals were excluded. 3×3 Pixels around the flux site were extracted to represent the flux tower (Wu et al., 2010).

The third MODIS product was the 8-day MODIS GPP product (MOD17A2, 1 km, collection 5.1), which is included in this study for model comparison. MODIS GPP is driven by daily MODIS land cover, f_{APAR}, leaf area index (LAI) and interpolated surface meteorology at 1 km for the global vegetated land surface (Zhao et al., 2006). This product is calculated as:

$$GPP = \varepsilon_{max} \times m(T_{min}) \times m(VPD) \times FPAR \times SWrad \times 0.45 \qquad (3)$$

where ε_{max} is the maximum LUE obtained from lookup tables on the basis of land cover type. The scalers $m(T_{min})$ and $m(VPD)$ reduce ε_{max} under unfavorable conditions of low temperature and high VPD. T_{min}, VPD and SWrad are obtained from large spatial-scale meteorological data sets that are available from the NASA Global Modeling and Assimilation Office (GMAO) (http://gmao.gsfc.nasa.gov/). Observations with quality flag of "good" and "best" were used for each site in 8-day interval and the mean value of the 3×3 pixels around the flux site was extracted for the comparison (Wu et al., 2012).

2.4. Global radiation data

To upscale the GR model and facilitate the model comparison with standard MODIS GPP, we downloaded the daily downward shortwave solar radiation flux from the National Center for

Table 1
Relationships between flux-measured GPP and EVI × PAR for each individual site.

Site ID	Variables			Site ID	Variables			Site ID	Variables		
Non-forest	Slope	Intercept	R^2	Deciduous forest	Slope	Intercept	R^2	Evergreen forest	Slope	Intercept	R^2
US-ARM	0.28	−5.37	0.39	US-HA1	0.54	−14.65	0.75	US-KS2	0.28	16.43	0.44
US-NE3	0.68	−22.00	0.60	US-BAR	0.45	−12.19	0.84	AU-TUM	0.54	5.97	0.66
DE-GEB	0.57	−8.85	0.76	US-MMS	0.46	−7.74	0.76	FR-PUE	0.20	13.10	0.42
DE-KLI	0.58	−11.10	0.80	US-MOZ	0.34	−1.64	0.77	IT-LEC	0.16	13.55	0.21
DK-RIS	0.46	1.41	0.76	US-SYV	0.48	−7.00	0.74	PT-ESP	0.26	17.32	0.20
NL-LUT	0.75	−12.67	0.73	US-WCR	0.59	−12.75	0.78	US-HO1	0.56	−11.53	0.78
UK-ESA	0.87	−9.28	0.77	BE-BRA	0.37	2.53	0.72	CA-NS3	0.39	−3.90	0.55
US-AUD	0.29	−6.40	0.27	DE-HAI	0.44	−1.61	0.76	US-ME2	0.56	−4.30	0.74
US-FPE	0.23	−0.89	0.36	DK-SOR	0.68	−1.83	0.80	US-NR1	0.38	−8.68	0.48
US-GOO	0.36	−0.65	0.51	FR-FON	0.54	0.42	0.57	CZ-BK1	0.60	1.32	0.68
US-VAR	0.32	−2.69	0.25	FR-HES	0.49	−8.42	0.78	DE-WET	0.68	3.83	0.67
US-WKG	0.31	−8.20	0.58	IT-COL	0.39	−5.91	0.83	FI-HYY	0.55	−1.82	0.78
DE-MEH	0.40	−3.38	0.88	IT-NON	0.49	8.24	0.62	FI-SOD	0.43	0.91	0.75
DK-LVA	0.48	8.63	0.48	IT-PT1	0.73	−9.34	0.93	FR-LBR	0.39	10.90	0.65
FR-LQ1	0.42	1.73	0.72	IT-RO1	0.38	−2.67	0.70	IT-BON	0.34	13.74	0.56
IL-AMP	0.24	5.00	0.40	IT-RO2	0.54	−4.60	0.64	IT-LAV	0.50	8.57	0.70
IT-MAL	0.40	9.64	0.45	CA-OAS	0.54	−6.84	0.79	IT-REN	0.45	1.53	0.57
NL-CA1	0.47	2.14	0.76					IT-SRO	0.44	11.22	0.54
NL-HOR	0.65	−1.60	0.88					NL-LOO	0.51	9.72	0.83
IT-PIA	0.22	3.12	0.15					SK-TAT	0.28	−2.11	0.76
CA-FEN	0.34	2.96	0.71					UK-GRI	0.42	5.57	0.50
US-TON	0.44	−5.89	0.61					CA-CA1	0.59	7.96	0.83
Au-HOW	0.47	−14.09	0.23					CA-CA3	0.37	3.72	0.76
ZA-KRU	0.47	−14.35	0.56					CA-CA2	0.40	−5.97	0.69
								CA-MAN	0.49	−3.54	0.61
								CA-TP1	0.22	−1.87	0.72
								CA-TP3	0.47	−9.15	0.72
								CA-OBS	0.55	−4.80	0.70
								CA-OJP	0.45	−5.75	0.62

Environmental Prediction (NCEP) reanalysis II data (http://www.esrl.noaa.gov/psd/data/gridded/data.ncep.reanalysis2.html). NCEP daily reanalysis II data provides the global radiation data divided into 192 × 94 Gaussian grids (~1.875°) and this dataset has been demonstrated to be appropriate for driving the MODIS global GPP algorithm (Zhao and Running, 2010). This dataset is an improved version of the NCEP reanalysis I model that fixes errors and updates parameterizations of physical processes and is thereby capable of capturing major changes in the surface climate anomalies (Betts et al., 2006). Radiation for each site was determined using the geographic location (latitude and longitude) of flux tower sites after bilinearly interpolating the NCEP data into 1 km grids.

2.5. The GR model

We used a remote sensing based greenness and radiation (GR) model for estimating GPP based on EVI and incoming PAR inputs (Gitelson et al., 2006). The underlying mechanism of this model lies in the correlation between the GPP and the total canopy chlorophyll content (Peng et al., 2011; Peng and Gitelson, 2011; Sakamoto et al., 2011). Therefore, vegetation indices that are proxies of total chlorophyll content together with incoming PAR can be used for GPP estimation. This GR model can be expressed as follows:

$$GPP = Slope(EVI \times PAR) + Intercept \qquad (4)$$

One of the uncertainties in the application of this model is the calibration with diverse ecosystems to determine the Slope and Intercept with respect to various PFTs. A previous effort in this aspect has shown promising results at monthly time step across North American flux sites (Wu et al., 2011). However, the feasibility of this model has not been demonstrated at shorter time scales of various ecosystems globally. In this analysis, the Slope and Intercept were determined by the following approach. We first calculated the relationship between GPP and EVI × PAR at each individual site. Then slopes and intercepts for sites of the same PFT were then empirically determined using site-level variables for each PFT. For data of individual site, we used all observations within a year (i.e., both leaf-on and leaf-off season) in later analysis.

3. Results

3.1. Relationship between measured GPP and EVI × PAR

We first compared the coarse resolution radiation data with measured radiation data for each PFT (Fig. 2). Close relationships were found between these two radiation datasets for each PFT ($R^2 > 0.85$, $p < 0.001$), assuring the use of the coarse resolution radiation dataset for both the standard MODIS GPP product and the GR model.

We then explored the relationship between flux-measured GPP and EVI × PAR for each PFT (Fig. 3). GPP grouped into three PFTs generally correlated well with EVI × PAR with R^2 of 0.54 ($p < 0.001$), 0.69 ($p < 0.001$) and 0.56 ($p < 0.001$) for NF, DF and EF sites, respectively. The slopes of each PFT imply that EVI × PAR would overestimate GPP without model calibration. We have also shown the potential of EVI × PAR in predicting GPP for each individual site (Table 1). For a single site data, we observed substantial differences in the R^2 of GPP vs. EVI × PAR relationship ranging from 0.15 ($p < 0.001$) for IT-PIA and 0.93 ($p < 0.001$) for IT-PT1. DF sites had the best results ($R^2 > 0.70$) and stable GPP and EVI × PAR relationships, which was indicated by the lowest coefficient of variation (CV = 11.5%) in R^2. The CV of R^2 for NF and EF sites were

26.0% and 38.1%, respectively, suggesting the largest variation in the ability of EVI × PAR to predict GPP for EF sites.

3.2. Model calibration and comparison with MODIS GPP

Modeling the slopes and intercepts of the relationships between GPP and EVI × PAR using remote sensing observations would
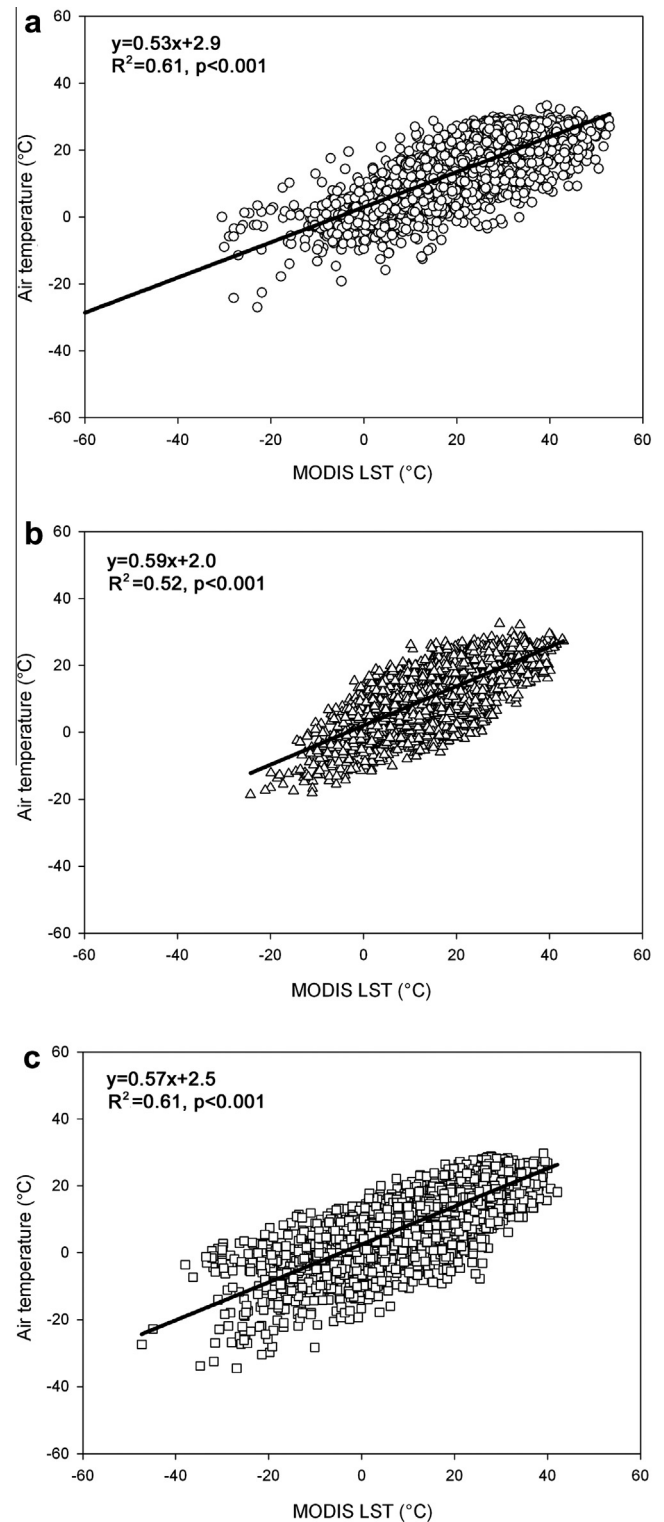

Fig. 4. Relationships between MODIS land surface temperature (LST) and the on site measured air temperature. The NF (○), DF (△), and EF (□) represent non-forest, deciduous forest, and evergreen forest ecosystems, respectively.

greatly favor its application across diverse ecosystems globally. To achieve this, we focused on the estimation of the slopes and intercepts for each PFT using statistical parameters from EVI and LST, both of which were shown to be useful in GPP model calibration (Sims et al., 2008; Wu et al., 2011).

To support the inclusion of the satellite LST, we first compared all LST with the flux-measured air temperature for each PFT (Fig. 4). Generally, MODIS LST is a reasonable proxy of air temperature with R^2 of 0.61 ($p < 0.001$), 0.52 ($p < 0.001$) and 0.61 ($p < 0.001$) for NF, DF and EF sites, respectively. MODIS LST tends to be lower than air temperature in the lower LST range while higher than air temperature in the high LST range. Such distribution has also been observed in previous study (Sims et al., 2008; Wu et al., 2010) (note that some of the same data were used in the present study, and thus these results are not fully independent).

Based on previous results of Wu et al. (2011), we try to explain the slopes and intercepts by a range of statistical variables of both EVI and LST. Statistical parameters of EVI included the minimum and maximum (EVI_{min} and EVI_{max}), the difference between minimum and maximum (dEVI), the average (EVI_{ave}) and the standard deviation of EVI (EVI_{sd}). Statistical parameters of LST were the average and standard deviation of LST (LST_{ave} and LST_{sd}). We found that the slopes and intercepts for each PFT can be explained by the single or combined forms of these statistical parameters (Fig. 5). For the NF sites, the slopes of each site were found to be correlated with dEVI ($R^2 = 0.52$, $p < 0.001$) and the variance in intercepts can be explained by dEVI × LST_{ave} ($R^2 = 0.47$, $p < 0.001$). For the DF sites, the slopes and intercepts were linear functions of EVI_{sd}/dEVI ($R^2 = 0.52$, $p = 0.001$) and LST_{ave}/EVI_{ave} ($R^2 = 0.53$, $p < 0.001$). Similarly, significant relationships were identified between the slopes and dEVI × LST_{ave} ($R^2 = 0.50$, $p < 0.001$) and between the intercepts and the LST_{ave}/EVI_{sd} ($R^2 = 0.60$, $p < 0.001$) of EF sites.

Using these empirical relationships, the GR model can then be calibrated and applied to predict GPP. To show the potential of the calibrated GR model, we applied it to predict GPP for each
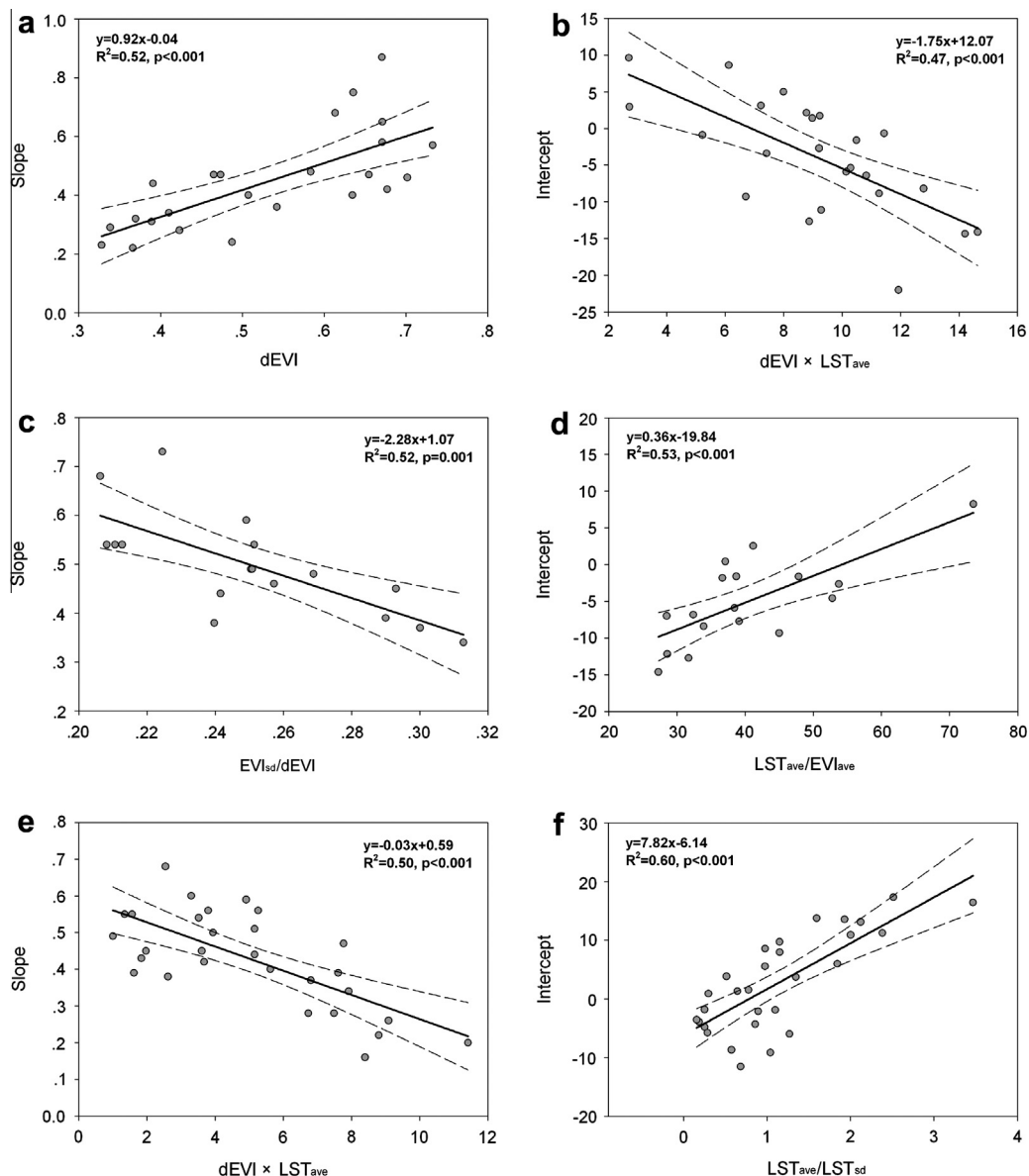

Fig. 5. Model calibration using enhanced vegetation index (EVI) and the land surface temperature (LST) for (a and b) non-forest, (c and d) deciduous forest and (e and f) evergreen forest sites. The Slope and Intercept are the regression coefficients in the relationship between flux GPP and EVI × PAR. dEVI, EVI_ave and EVI_sd represent the difference between maximum and minimum EVI, the average value of EVI, and the standard deviation of EVI, respectively. LST_ave and LST_sd are the average value and the standard deviation of LST, respectively. Points represent data of each site. Solid and dash lines represent regression and 95% confidence, respectively.

PFT and included the MODIS GPP for comparison (Fig. 6). MODIS GPP generally showed moderate performances in GPP estimations for the three PFTs with R^2 of 0.42 ($p < 0.001$), 0.42 ($p < 0.001$) and 0.52 ($p < 0.001$) for NF, DF and NF sites, respectively. The root mean square error (RMSE) of estimated GPP ranged from 16.9 g C m^{-2} 8 - d^{-1} for EF sites to 27.4 m^{-2} 8 d^{-1} for DF sites. Furthermore, MODIS GPP was observed to be higher than flux GPP at the low end of the range while lower than flux GPP at the upper end of the GPP range for all PFTs (note the extent may differ among PFTs). This pattern has been reported in previous analysis of both site level (Harris and Dash, 2010; Wu et al., 2011) and regional evaluations (Sjöström et al., 2011). Improper characterization of shaded leaves in dense canopies by the MODIS GPP algorithm was identified as the main reason for this pattern (Cheng et al., 2010; Wu et al., 2012; Zhang et al., 2012; Chen et al., 2012). Using the calibrated GR model, we observed improved GPP estimates for all PFTs with all R^2 above 0.60 ($p < 0.001$). DF sites performed the best with R^2 of 0.72 ($p < 0.001$) and a 30% improvement in the RMSE with a value of 19.1 m^{-2} 8 d^{-1} compared to MODIS GPP product. The slopes

for all of the regressions were close to unity, indicating the robustness of the model calibration approach.

We also compared the calibration results with standard MODIS GPP product at each site and the slopes, intercepts and R^2 for both models were calculated (not shown here for brevity). Significant correlations ($p < 0.001$) were found between GR modeled GPP and flux-measured GPP for all sites. For MODIS GPP, three sites have not shown statistically significant correlations with flux-measured GPP (IT-RO2, IT-LEC and IT-BON). GR model produced comparable results with MODIS GPP product for NF and EF sites. The GR model performed better in most of DF sites compared to standard MODIS GPP product. We further calculated the average slopes and intercepts as well as their standard deviations for each PFT (Fig. 7). The average slopes (standard deviation) of MODIS GPP were 1.29 (0.52), 1.41 (0.46) and 0.92 (0.23) for NF, DF and EF sites, respectively, implying MODIS GPP would have underestimated results for ND and DF sites. But for EF sites, such underestimation was not that evident, probably due to a lower range of GPP for EF sites. The average (standard deviation) slopes of the calibrated
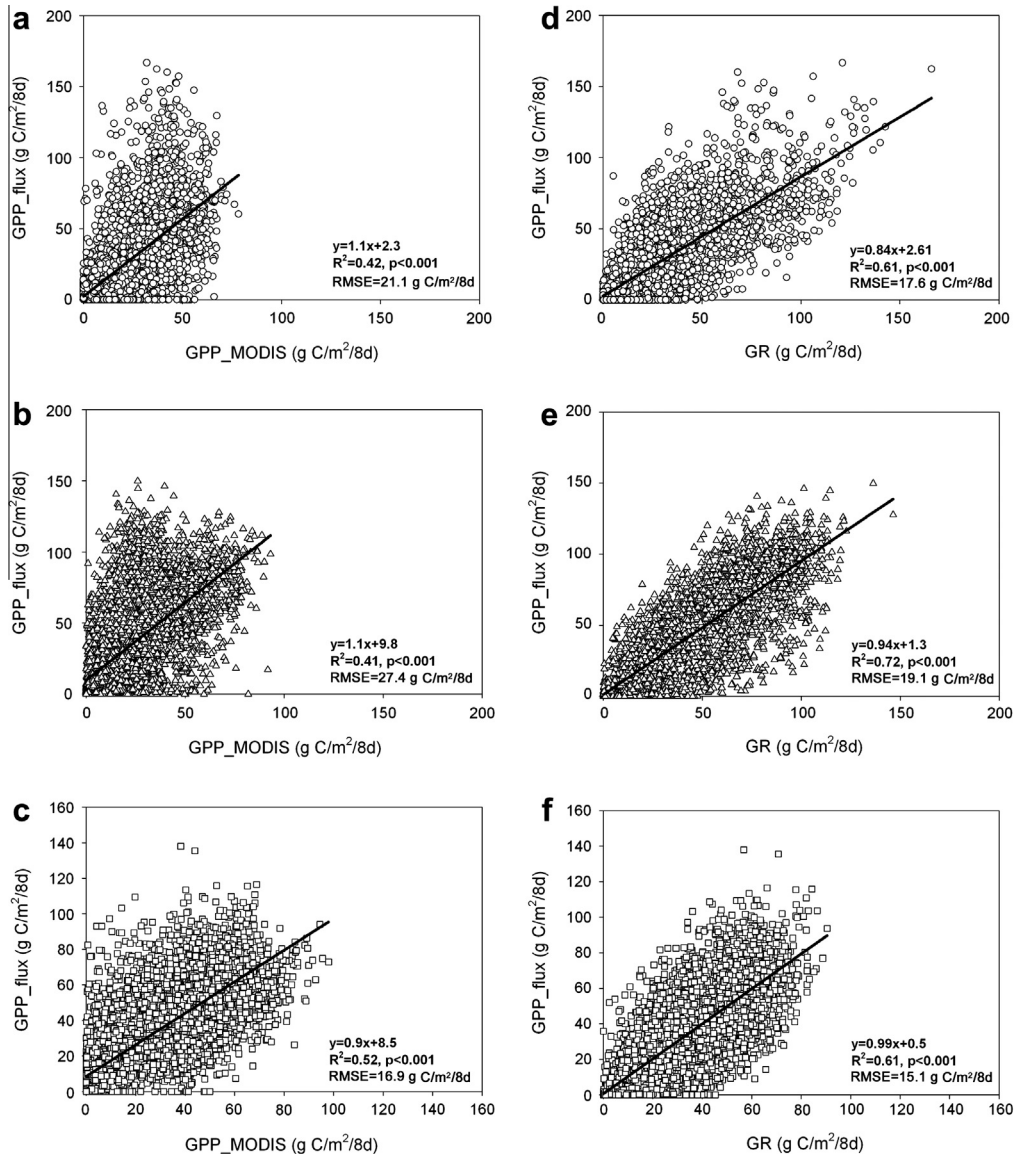

Fig. 6. MODIS 8-day gross primary production (GPP) in (a) non-forest (○), (b) deciduous forest (△), and (c) evergreen forest (□) sites. Modeled GPP using the greenness and radiation model (GR) in (d) non-forest (○), (e) deciduous forest (△), and (f) evergreen forest (□) sites. Solid and dash lines represent the regression and 1:1 lines, respectively.
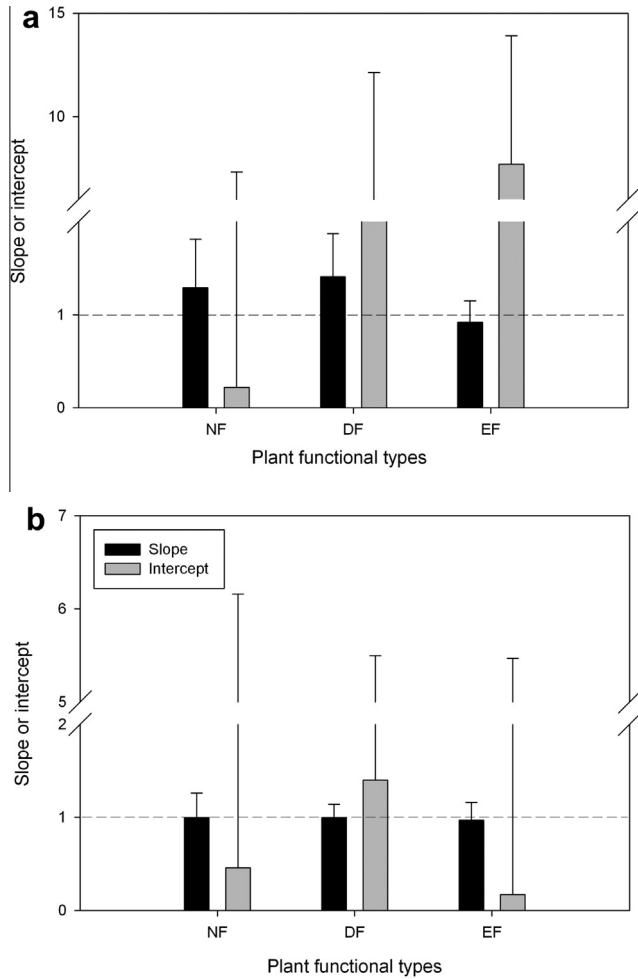
Fig. 7. Comparison between the average slopes and intercepts from individual sites for (a) MODIS GPP and (b) GR model estimated GPP in three plant functional types. NF, DF and EF represent non-forest deciduous forest, and evergreen forest ecosystems, respectively. The error bar indicates the standard deviation (sd) of each variable for all sites of the same plant functional type and the dash lines indicate slopes of 1.

GR model for the three PFTs were 1.00 (0.26), 1.00 (0.14) and 0.97 (0.19), indicating improved GPP estimates and model stability.

3.3. Latitudinal patterns of model performance

Grouping vegetation types in different ecoregions may add complexity as similar vegetation type may be growing under different environmental conditions. We therefore explored the model performance (i.e., R^2 between GR modeled and flux-measured GPP) as a function of latitudinal gradient which would show how regional climates (temperature and rain) affect the GR model performance.

Since there were only three sites in the Southern Hemisphere, here we only focused on the Northern sites (Fig. 8). We found significant correlations between model performance and latitude with R^2 of 0.38 ($p = 0.002$) and 0.25 ($p = 0.015$) for NF and EF sites, respectively. This indicates that GR model can generally provide better GPP estimates for sites located at higher latitudes for these two PFTs. In comparison, DF sites did not show this pattern, suggesting that the GR model is more applicable for DF sites and model performance may be independent on regional climate. These show that we may expect a combined effect of both PFT and regional climate on the model performance.
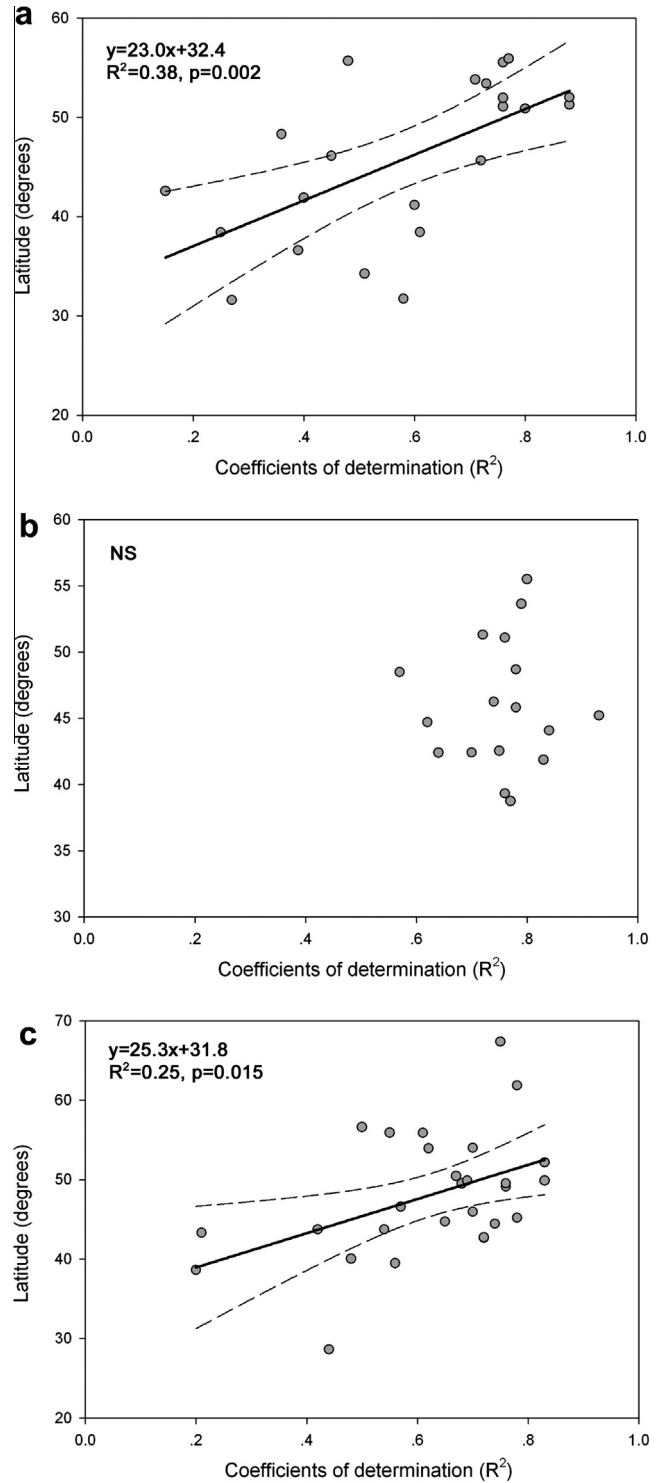

Fig. 8. Latitudinal pattern of mode performance as indicated by the coefficients of determination (R^2) between flux-measured GPP and GR modeled GPP for (a) non-forest sites, (b) deciduous forest sites, and (c) evergreen forest sites. Solid and dash lines represent regression and 95% confidence, respectively.

4. Discussion

4.1. The reason of using radiation to capture short-term GPP variations

The GR model showed promising results for estimating 8-day GPP for different PFTs. Canopy greenness (i.e., EVI) and radiation act as two factors regulating the model performance. A single

vegetation index (e.g., EVI) only provides a measure of canopy greenness and it cannot capture the influences of short-term meteorological variables on GPP, especially the variations in temperature. This is the main reason limiting the use of a single index for estimating short-term GPP. Previous analysis by Sakamoto et al. (2011) demonstrated that daily GPP cannot be explained by a single WDRVI index but a combination with radiation capturing certain short-term meteorological variations would help to interpret GPP. To explain this, we explored the relationship between gridded radiation and the flux-measured air temperature for all observations (Fig. 9). We found that the air temperatures of all PFTs were highly correlated with the gridded radiation, indicating that the requirement of independent temperature may not be necessary for the GR model. This probably is the reason for the wide applicability of the GR model for such diverse ecosystems in our analysis, especially in capturing the 8-day GPP variations. We also suggest that it is this potential that explains the results of GPP estimation using the GR model even at the daily step (Peng and Gitelson, 2012). One however should note that our analysis may only support the potential of radiation in capturing temperature based stress, which may be not true for water (e.g., soil moisture) stress (e.g., low precision at US-VAR).

4.2. Physiologically-based interpretation of calibration process

Our previous evaluation of the GR model to estimate monthly GPP in the growing season of several North America vegetation ecosystems indicated good performances (Wu et al., 2011). However, the underestimation of high GPP and the overestimation low GPP was also shown to be the main limitation of the GR model. The measured GPP from several non-growing season observations is very low (close to zero) while the GR model considerably overestimated the GPP, indicating both regression slopes and intercepts should be calibrated carefully. For NF and DF sites, the regression slopes were correlated with EVI-related parameters, implying that the dynamical ranges of canopy greenness were the main factor driving the model performances. By comparison, for EF sites, the variation in canopy greenness is very small and therefore it may not be that important. In such situations, the temperature may become an important factor in regulating GPP. Accordingly, we found no correlation between EVI-related parameters and the regression slopes while single LST_{ave} can explain as much as 37% variances ($p < 0.001$, data not shown here for brevity). Therefore, an integrated form of $dEVI \times LST_{ave}$ has been found to have the best potential in explaining slopes of EF sites. For all PFTs, determinations of intercepts were achieved through the inclusion of MODIS LST. The underlying mechanism probably is that cold temperature mainly suppresses GPP to zero while the algorithm ($EVI \times PAR$) still gives estimates above zero since there is abundant PAR in most period of the non-growing season and EF have relatively consistent EVI values throughout the year. Therefore, inclusion of MODIS LST would help to remedy this difference and thus to calibrate the model.

The interesting aspect of our analysis is the physiological interpretation of slopes and intercepts. According to the Monteith logic, GPP is linearly correlated with LUE and APAR. Since the GR model is based on the relationships between total chlorophyll content and GPP, it does not belong to the LUE model. Therefore, the slope here may not be interpreted as directly equivalent to LUE value in LUE-based GPP model. The intercept may represent the overestimation or underestimation of GPP using the GR model since it is obtained when x-axis (i.e., GR model prediction) is zero, showing the bias compared to the corresponding flux measured GPP value on the y-axis.
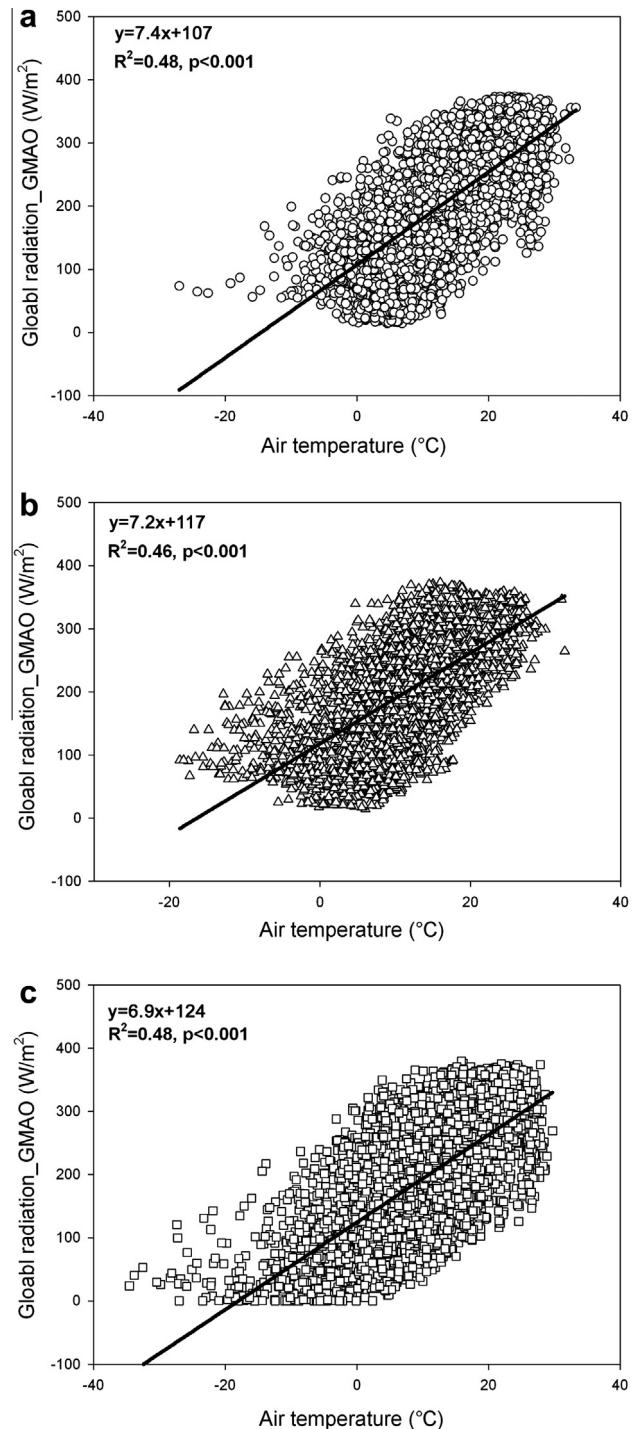

Fig. 9. Relationships between flux-measured air temperature and global radiation acquired from the National Center for Environmental Prediction (NCEP) reanalysis II data. The NF (○), DF (△), and EF (□) represent non-forest, deciduous forest, and evergreen forest ecosystems, respectively.

5. Conclusions

Using 70 global flux sites, we have demonstrated the potential of a simple remote sensing based GR model for predicting 8-day GPP across diverse vegetation ecosystems globally. This model is entirely driven by remote sensing observations (i.e., EVI and LST) and global coarse resolution radiation data. Model calibration was achieved by empirical correlations of statistical parameters

derived from EVI and LST. The calibrated model showed improved GPP estimates compared to the standard MODIS GPP product.

Previous analysis of this model at monthly time step may only be an indicator of plant phenology and potentially cannot capture short-term GPP variations due to regional climate variations (Wu et al., 2011). However, with the current evaluation, it is suggested that the GR model can capture short-term GPP variations through the combination of vegetation index and radiation data. Such results are useful in developing new GPP algorithms that are entirely based on easily available remote sensing and coarse resolution meteorological observations to circumvent the difficulties in acquiring ground data globally. Our evaluation also supports the great potential of the MODIS land surface products in monitoring ecosystem processes (Ryu et al., 2011). A further investigation will include mapping the spatial patterns of regional GPP, which would provide great help for the estimation of global C sequestration.

Acknowledgments

Appendix A. Supplementary material

Supplementary data associated with this article can be found, in the online version, at http://dx.doi.org/10.1016/j.isprsjprs.2013.10.015.

References

Barr, A.G., Black, T.A., Hogg, E.H., Kljun, N., Morgenstern, K., Nesic, Z., 2004. Interannual variability in the leaf area index of a boreal aspen-hazelnut forest in relation to net ecosystem production. Agric. For. Meteorol. 126 (3–4), 237–255.

Beer, C., Reichstein, M., Tomelleri, E., Ciais, P., Jung, M., Carvalhais, N., Rödenbeck, C., Arain, M.A., Baldocchi, D., Bonan, G.B., Bondeau, A., Cescatti, A., Lasslop, G., Lindroth, A., Lomas, M., Luyssaert, S., Margolis, H., Oleson, K.W., Roupsard, O., Veenendaal, E., Viovy, N., Williams, C., Ian Woodward, F., Papale, D., 2010. Terrestrial gross carbon dioxide uptake: global distribution and covariation with climate. Science 329 (5993), 834–838.

Betts, A.K., Zhao, M., Dirmeyer, P.A., Beljaars, A.C.M., 2006. Comparison of ERA40 and NCEP/DOE near-surface data sets with other ISLSCP-II data sets. J. Geophys. Res. 111, D22S04. http://dx.doi.org/10.1029/2006JD007174.

Chen, J.M., Mo, G., Pisek, J., Liu, J., Deng, F., Ishizawa, M., Chan, D., 2012. Effects of foliage clumping on the estimation of global terrestrial gross primary productivity. Global Biogeochem. Cycles 26, GB1019. http://dx.doi.org/10.1029/2010GB003996.

Cheng, Y.B., Middleton, E.M., Huemmrich, K.F., Zhang, Q., Campbell, P.K.E., Corp, L.A., Russ, A.L., Kustas, W.P., 2010. Utilizing in situ directional hyperspectral measurements to validate bio-indicator simulations for a corn crop canopy. Ecol. Inform. 5 (5), 330–338.

Coops, N.C., Black, T.A., Jassal, R.S., Trofymow, J.A., Morgenstern, K., 2007. Comparison of MODIS, eddy covariance determined and physiologically

modeled gross primary production (GPP) in a Douglas-fir forest stand. Remote Sens. Environ. 107 (3), 385–401.

Dash, J., Curran, P.J., 2004. The MERIS terrestrial chlorophyll index. Int. J. Remote Sens. 25 (23), 5403–5413.

Desai, A.R., Richardson, A.D., Moffat, A.M., Kattge, J., Hollinger, D.Y., Barr, A., Falge, E., Noormets, A., Papale, D., Reichstein, M., Stauch, V.J., 2008. Cross site evaluation of eddy covariance GPP and RE decomposition techniques. Agric. For. Meteorol. 148 (6–7), 821–838.

Field, C.B., Behrenfeld, M.J., Randerson, J.T., Falkowski, P., 1998. Primary production of the biosphere: integrating terrestrial and oceanic components. Science 281 (5374), 237–240.

Gamon, J.A., Serrano, L., Surfus, J.S., 1997. The photochemical reflectance index: an optical indicator of photosynthesis radiation use efficiency across species, functional types, and nutrient levels. Oecologia 112 (4), 492–501.

Gitelson, A.A., 2004. Wide dynamic range vegetation index for remote quantification of biophysical characteristics of vegetation. J. Plant Physiol. 161 (2), 165–173.

Gitelson, A.A., Viña, A., Masek, J.G., Verma, S.B., Suyker, A.E., 2008. Synoptic monitoring of gross primary productivity of maize using Landsat data. IEEE Geosci. Remote Sens. Lett. http://dx.doi.org/10.1109/LGRS.2008.915598.

Gitelson, A.A., Viña, A., Verma, S.B., Rundquist, D.C., Arkebauer, T.J., Keydan, G., Leavitt, B., Ciganda, V., Burba, G.G., Suyker, A.E., 2006. Relationship between gross primary production and chlorophyll content in crops: implications for the synoptic monitoring of vegetation productivity. J. Geophys. Res. 111, D08S11. http://dx.doi.org/10.1029/2005JD006017.

Hall, F.G., Hilker, T., Coops, N.C., 2011. PHOTOSYNSAT, photosynthesis from space: theoretical foundations of a satellite concept and validation from tower and spaceborne data. Remote Sens. Environ. 115 (8), 1918–1925.

Harris, A., Dash, J., 2010. The potential of the MERIS terrestrial chlorophyll index for carbon flux estimation. Remote Sens. Environ. 114 (8), 1856–1862.

Hilker, T., Coops, N.C., Hall, F.G., Black, T.A., Wulder, M.A., Nesic, Z., Krishnan, P., 2008a. Separating physiologically and directionally induced changes in PRI using BRDF models. Remote Sens. Environ. 112 (6), 2777–2788.

Hilker, T., Coops, N.C., Wulder, M.A., Black, T.A., Guy, R.D., 2008b. The use of remote sensing in light use efficiency based models of gross primary production: a review of current status and future requirements. Sci. Total Environ. 404 (2–3), 411–423.

Huete, A., Didan, K., Miura, T., Rodriguez, E.P., Gao, X., Ferreira, L.G., 2002. Overview of the radiometric and biophysical performance of the MODIS vegetation indices. Remote Sens. Environ. 83 (1–2), 195–213.

Kalfas, J.L., Xiao, X., Vanegas, D.X., Verma, S.B., Suyker, A.E., 2011. Modeling gross primary production of irrigated and rain-fed maize using MODIS imagery and CO₂ flux tower data. Agric. For. Meteorol. 151 (12), 1514–1528.

Kanniah, K.D., Beringer, J., Hutley, L.B., Tapper, N.J., Zhu, X., 2009. Evaluation of collections 4 and 5 of the MODIS gross primary productivity product and algorithm improvement at a tropical savanna site in northern Australia. Remote Sens. Environ. 113 (9), 1808–1822.

Monteith, J.L., 1972. Solar radiation and production in tropical ecosystems. J. Appl. Ecol. 9 (3), 747–766.

Mu, Q., Zhao, M., Running, S.W., 2011. Improvements to a MODIS global terrestrial evapotranspiration algorithm. Remote Sens. Environ. 115 (8), 1781–1800.

Papale, D., Valentini, A., 2003. A new assessment of European forests carbon exchange by eddy fluxes and artificial neural network spatialization. Glob. Change Biol. 9 (4), 525–535.

Papale, D., Reichstein, M., Aubinet, M., Canfora, E., Bernhofer, C., Kutsch, W., Longdoz, B., Rambal, S., Valentini, R., Vesala, T., Yakir, D., 2006. Towards a standardized processing of net ecosystem exchange measured with eddy covariance technique: algorithms and uncertainty estimation. Biogeosciences 3 (4), 571–583.

Peng, Y., Gitelson, A.A., 2012. Remote estimation of gross primary productivity in soybean and maize based on total crop chlorophyll content. Remote Sens. Environ. 117, 440–448.

Peng, Y., Gitelson, A.A., 2011. Application of chlorophyll-related vegetation indices for remote estimation of maize productivity. Agric. For. Meteorol. 151 (9), 1267–1276.

Peng, Y., Gitelson, A.A., Keydan, G., Rundquist, D.C., Moses, W., 2011. Remote estimation of gross primary production in maize and support for a new paradigm based on total crop chlorophyll content. Remote Sens. Environ. 115 (4), 978–989.

Reichstein, M., Falge, E., Baldocchi, D., Papale, D., Aubinet, M., Berbigier, P., Bernhofer, C., Buchmann, N., Gilmanov, T., Granier, A., Grunwald, T., Havrankova, K., Ilvesniemi, H., Janous, D., Knohl, A., Laurila, T., Lohila, A., Loustau, D., Matteucci, G., Meyers, T., Miglietta, F., Ourcival, J.M., Pumpanen, J., Rambal, S., Rotenberg, E., Sanz, M., Tenhunen, J., Seufert, G., Vaccari, F., Vesala, T., Yakir, D., Valentini, R., 2005. On the separation of net ecosystem exchange into assimilation and ecosystem respiration: review and improved algorithm. Glob. Change Biol. 11 (9), 1424–1439.

Rouse, J.W., Haas, R.H., Schell, J.A., Deering, D.W., Harlan, J.C., 1974. Monitoring the vernal advancements and retrogradation of natural vegetation. In: NASA/GSFC. Final Report. Greenbelt, MD, USA, pp. 1–137.

Running, S.W., Nemani, R.R., Heinsch, F.A., Zhao, M., Reeves, M., Hashimoto, H., 2004. A continuous satellite-derived measure of global terrestrial primary production. Bioscience 54 (6), 547–560.

Ryu, Y., Baldocchi, D.D., Kobayashi, H., van Ingen, C., Li, J., Black, T.A., Beringer, J., van Gorsel, E., Knohl, A., Law, B.E., Roupsard, O., 2011. Integration of MODIS land and atmosphere products with a coupled-process model to estimate gross primary

productivity and evapotranspiration from 1 km to global scales. Global Biogeochemical Cycles, 25(GB4017).http://dx.doi.org/10.1029/2011GB004053.

Sakamoto, T., Gitelson, A.A., Wardlow, B.D., Verma, S.B., Suyker, A.E., 2011. Estimating daily gross primary production of maize based only on MODIS WDRVI and shortwave radiation data. Remote Sens. Environ. 115 (12), 3091–3101.

Sims, D.A., Rahman, A.F., Cordova, V.D., El-Masri, B.Z., Baldocchi, D.D., Bolstad, P.V., Flanagan, L.B., Goldstein, A.H., Hollinger, D.Y., Misson, L., Monson, R.K., Oechel, W.C., Schmid, H.P., Wofsy, S.C., Xu, L., 2008. A new model of gross primary productivity for North American ecosystems based solely on the enhanced vegetation index and land surface temperature from MODIS. Remote Sens. Environ. 112 (4), 1633–1646.

Sjöström, M., Ardö, J., Arneth, A., Boulain, N., Cappelaere, B., Eklundh, L., de Grandcourt, A., Kutsch, W.L., Merbold, L., Nouvellon, Y., Scholes, R.J., Schubert, P., Seaquist, J., Veenendaal, E.M., 2011. Exploring the potential of MODIS EVI for modeling gross primary production across African ecosystems. Remote Sens. Environ. 115 (4), 1081–1089.

Turner, D.P., Urbanski, S., Bremer, D., Wofsy, S.C., Meyers, T., Gower, S.T., Gregory, M., 2003. A cross-biome comparison of daily light use efficiency for gross primary production. Glob. Change Biol. 9 (3), 383–395.

Vermote, E.F., El Saleous, N., Justice, C.O., Kaufman, Y.J., Privette, J.L., Remer, L., Roger, J.C., Tanré, D., 1997. Atmospheric correction of visible to middle-infrared EOS-MODIS data over land surfaces: background, operational algorithm and validation. J. Geophys. Res. 102 (D14), 17131–17141.

Wan, Z., 2008. New refinements and validation of the MODIS land-surface temperature/emissivity products. Remote Sens. Environ. 112 (1), 59–74.

Wang, H., Jia, G., Fu, C., Feng, J., Zhao, T., Ma, Z., 2010. Deriving maximal light use efficiency from coordinated flux measurements and satellite data for regional gross primary production modeling. Remote Sens. Environ. 114 (10), 2248–2258.

Wu, C., Chen, J.M., Huang, N., 2011. Predicting gross primary production from the enhanced vegetation index and photosynthetically active radiation: evaluation and calibration. Remote Sens. Environ. 115 (12), 3424–3435.

Wu, C., Chen, J.M., Desai, A.R., Hollinger, D.Y., Arain, M.A., Margolis, H.A., Gough, C.M., Staebler, R.M., 2012. Remote sensing of canopy light use efficiency in temperate and boreal forests of North America using MODIS imagery. Remote Sens. Environ. 118, 60–72.

Wu, C., Munger, J.W., Niu, Z., Kuang, D., 2010. Comparison of multiple models for estimating gross primary production using MODIS and eddy covariance data in Harvard Forest. Remote Sens. Environ. 114 (12), 2925–2939.

Wu, C., Niu, Z., Tang, Q., Huang, W., Rivard, B., Feng, J., 2009. Remote estimation of gross primary production in wheat using chlorophyll-related vegetation indices. Agric. For. Meteorol. 149 (6–7), 1015–1021.

Xiao, X.M., Boles, S., Liu, J.Y., Zhuang, D.F., Frolking, S., Li, C.S., Salas, W., Moore, B., 2005. Mapping paddy rice agriculture in southern China using multi-temporal MODIS images. Remote Sens. Environ. 95 (4), 480–492.

Xiao, X., Boles, S., Frolking, S., Li, C., Babu, J.Y., Salas, W., Berrien Moore, I.I.I., 2006. Mapping paddy rice agriculture in South and Southeast Asia using multi-temporal MODIS images. Remote Sens. Environ. 100 (1), 95–113.

Yuan, W., Liu, S., Yu, G., Bonnefond, J., Chen, J., Davis, K., Desai, A.R., Goldstein, A.H., Gianelle, D., Rossi, F., Suyker, A.E., Verma, S.B., 2010. Global estimates of evapotranspiration and gross primary production based on MODIS and global meteorology data. Remote Sens. Environ. 114 (7), 1416–1431.

Zhang, Q., Middleton, E.M., Margolis, H.A., Drolet, G.G., Barr, A.A., Black, T.A., 2009. Can a satellite-derived estimate of the fraction of PAR absorbed by chlorophyll (FAPAR$_{chl}$) improve predictions of light-use efficiency and ecosystem photosynthesis for a boreal Aspen forest? Remote Sens. Environ. 113 (4), 880–888.

Zhang, F., Chen, J.M., Chen, J., Gough, C.M., Martin, T., Dragoni, D., 2012. Evaluating spatial and temporal patterns of MODIS GPP over the conterminous U.S. against flux measurements and a process model. Remote Sens. Environ. 124, 717–729.

Zhao, M., Running, S.W., 2010. Drought-induced reduction in global terrestrial net primary production from 2000 through 2009. Science 329 (5994), 940–943.

Zhao, M., Heinsch, F.A., Nemani, R.R., Running, S.W., 2005. Improvement of the MODIS terrestrial gross and net primary production global dataset. Remote Sens. Environ. 95 (2), 164–176.

Zhao, M., Running, S.W., Nemani, R.R., 2006. Sensitivity of Moderate Resolution Imaging Spectroradiometer (MODIS) terrestrial primary production to the accuracy of meteorological reanalyses. J. Geophys. Res. 111, G01002. http://dx.doi.org/10.1029/2004JG000004.